Journal of Communications Technology and Electronics, Vol. 47, No. 12, 2002, pp. 1387–1397. From Radiotekhnika i Elektronika, Vol. 47, No. 12, 2002, pp. 1517–1528.

NEW ELECTRONIC SYSTEMS AND UNITS

Selective and Wavelength Transparent Optical Add-Drop Multiplexer Based on Fiber Bragg Gratings[1]

P. S. Andre, A. N. Pinto, J. L. Pinto, T. Almeida, and M. Pousa

Received June 20, 2000

Abstract—A configurable optical add-drop multiplexer (OADM) based on fiber Bragg gratings is reported. Dynamical selection of the add-drop or pass-through functionality is realized according to the control of an optical switch. OADM performance measurements in a 70-km, 3×2.5-Gb/s channel wavelength division multiplexing (WDM) network are reported. The wavelength tuning capacity for the OADM is studied.

I. INTRODUCTION

Wavelength division multiplexing (WDM) technologies are rapidly maturing to satisfy the substantial increase in telecommunications network capacity. The tremendous rate in traffic growth due to the demands for multimedia services will urge the development of wavelength routing technologies in place of point-to-point multiwavelength transmission. Especially, optical add-drop multiplexers (OADM) are expected to play an important role in enabling greater connectivity and flexibility in WDM networks.

A WDM network with a static OADM may provide a reliable, cost-effective, and scalable network since the static OADM is based on low-loss, low-cost, passive devices and does not need any power supply. A wavelength tunable OADM, giving access to all the wavelengths of the WDM signals, provides more flexibility to satisfy reconfiguration requirements and to enhance network protection.

The OADM is used for selectively dropping and inserting optical signals into a transparent DWDM network. Several wavelength OADMs have been proposed based on arrayed waveguide gratings (AWG) [1], Fabry-Perot filters [2], a combination of dielectric thin-film MUX and DEMUX [3], and Bragg gratings written in Mach-Zhender interferometers [4]. In this work, we propose a more simple, cost effective, flexible, easily upgradable, and transparent configuration using a fiber Bragg grating (FBG), an optical circulator, a power combiner, and a mechanical-optical switch [5].

A fundamental difficulty of wavelength routing is the crosstalk from neighboring inputs, causing severe degradation in system performance. In this work, we will describe the model used to the crosstalk; the performance of a WDM network with the OADM is reported and the tunability of the FBG discussed. Finally, the conclusions of the work will be presented.

II. CROSSTALK

Due to the wavelength reuse scheme, crosstalk is a major problem. The crosstalk arises from coherent mixing of a received signal with a crosstalk wave on the photodetector, originating an interference beat noise locally at the receiver. In the case of this OADM configuration, a heterodyne crosstalk is induced between the drop signal and the leakage of the remaining input signals at different wavelengths. The power penalty can be calculated by, the following equation [6], based on the eye closure:

$$P_{\mathrm{p}} = -10\log(1 - X), \tag{1}$$

where X is the crosstalk ratio.

Another type of crosstalk is the homodyne crosstalk induced between the add signal and the leakage of the

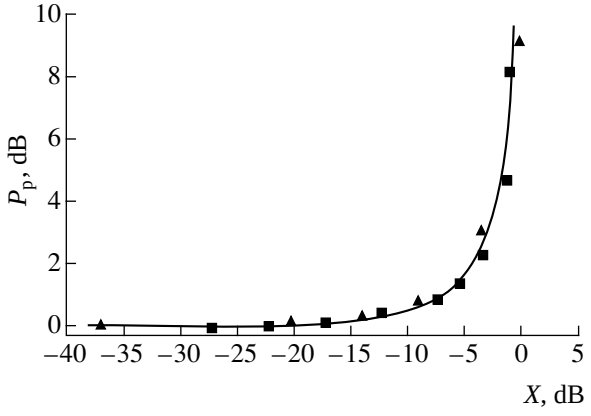

Fig. 1. Power penalty due to heterodyne crosstalk.

[1] This article was submitted by the authors in English.

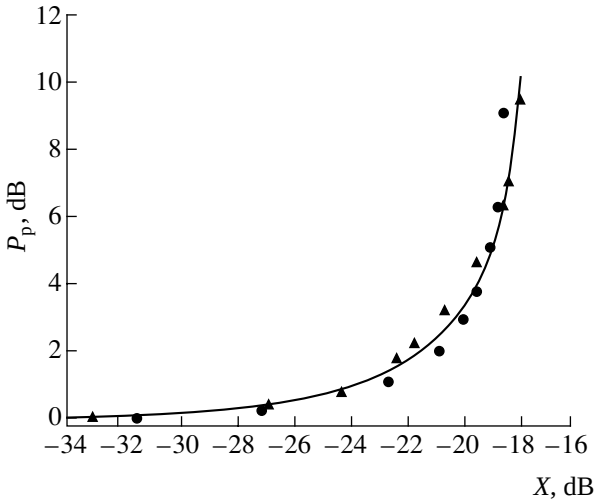

Fig. 2. Power penalty due to homodyne crosstalk.

drop signal at the same wavelength. The power penalty due to this crosstalk can be calculated by the following equation, assuming the worst-case situation, where the states of polarization (SOP) from the interference signals are the same and when the decision threshold is set at the optimized value to minimize the bit error rate (BER) [6]:

$$P_p = -10\log(1 - Q^2 X), \quad (2)$$

where Q indicates the signal-to-noise ratio (SNR). In this case, we consider a small crosstalk value, and consequently the noise will have a Gaussian probability density function. Therefore, Q will be equal to 6 for a $E = 10^{-9}$ BER. This power penalty will be far larger than the heterodyne power penalty and may limit the ability to cascade many OADMs simultaneously. The homodyne crosstalk can be reduced by eliminating reflections from connectors and components and by using a FBG with high reflectivity. To investigate whether this approximated model is precise in describing the crosstalk, we implemented an experimental setup to measure the power penalty due to the homodyne and heterodyne crosstalk for an amplitude shift keying direct detection system, externally modulated at

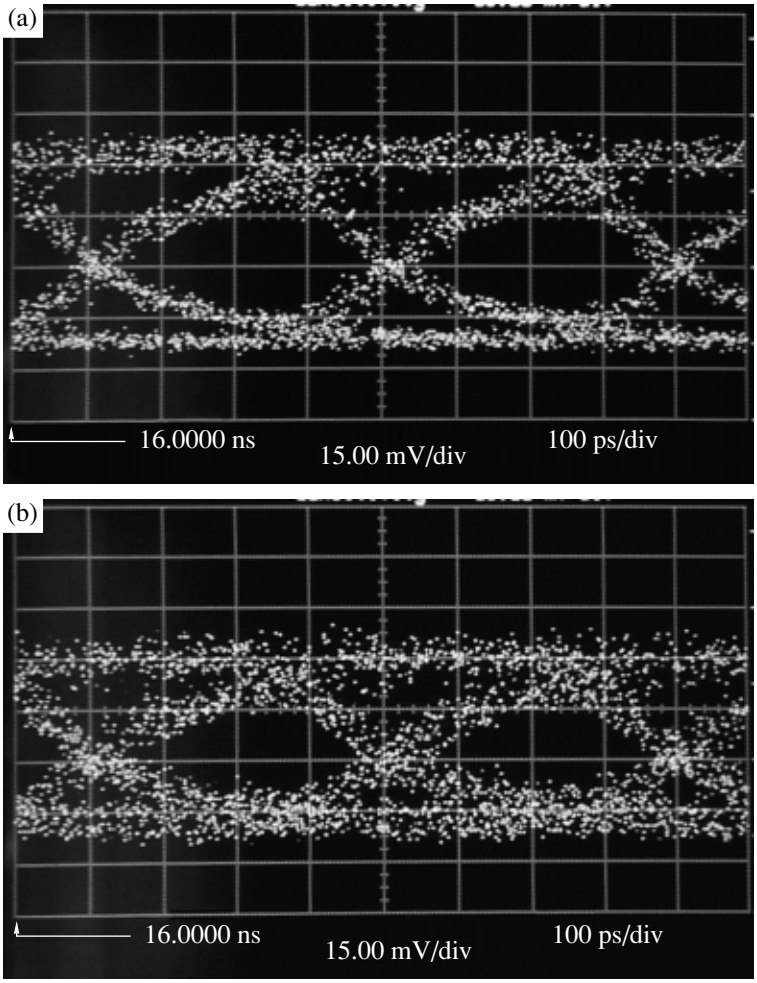

Fig. 3. Eye diagram for the detected channel in the presence of heterodyne crosstalk. (a) –40 and (b) –5 dB of crosstalk ratio.

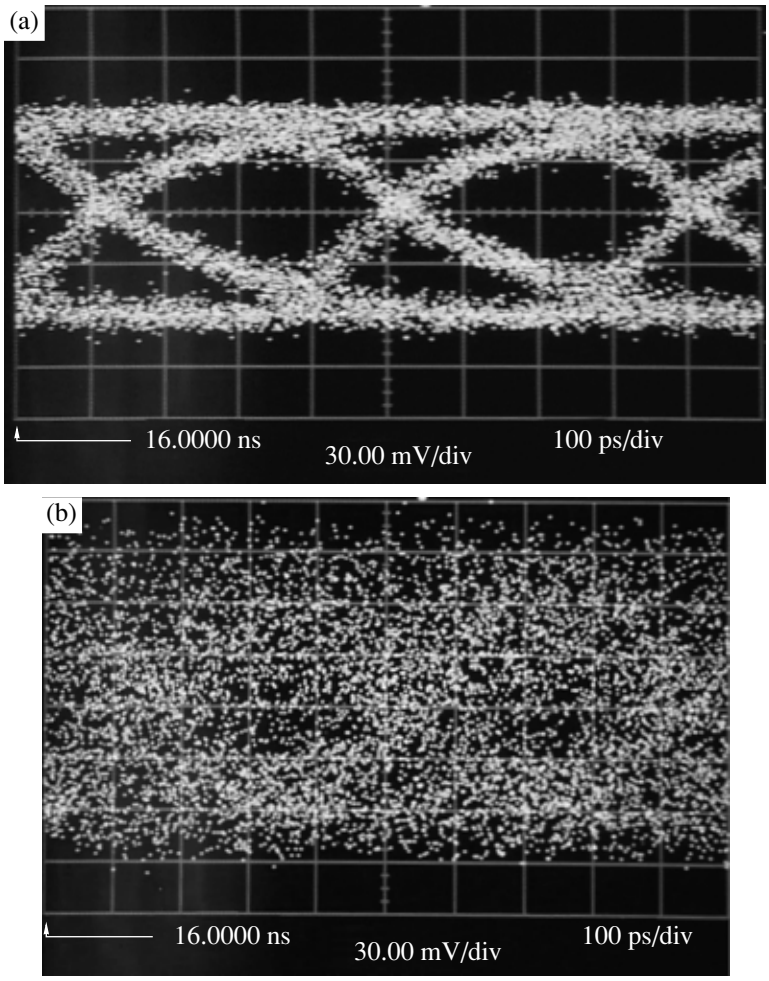

Fig. 4. Eye diagram for the detected channel in the presence of homodyne crosstalk. (a) –40 and (b) –5 dB of crosstalk ratio.

2.48832 Gbit/s. The experimental results were compared with simulated results obtained from a photonic transmission simulator (PTDS from Virtual Photonics (c)) and with the analytical expression from Eqs. (1) and (2) for the heterodyne and the homodyne crosstalk, respectively.

Figure 1 shows the results for the heterodyne crosstalk; in this case, two channels with a wavelength separation of 200 GHz from the detected channel were used as crosstalk waves.

Figure 2 shows the results for the homodyne crosstalk, where a channel with the same wavelength as the detected channel was used as crosstalk wave.

It can be seen that the analytical model used to predict the power penalty due to crosstalk, the measured values and simulated result are in agreement within experimental uncertainties. Usually, with the same crosstalk intensity, the effect of homodyne crosstalk is usually more than one order larger than that caused by the heterodyne crosstalk. These results can be seen in Figs. 3 and 4, where the diagram from the detected signal with –5 dB of homodyne and heterodyne crosstalk are compared; the eye diagram for a crosstalk ratio of –40 dB is also plotted.

III. OADM

The basic architecture of the OADM node and the WDM system used to test it are displayed in Fig. 5. It consists of fiber Bragg gratings, an optical circulator, a power combiner, and an optical switch. At first, *N* multiplexed wavelengths are led to the Bragg grating

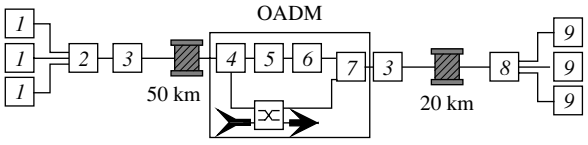

Fig. 5. Schematic of the OADM and experimental transmission network. (*1*) Optical transmitter, (*2*) optical switch, (*3*) optical amplifier, (*4*) circulator, (*5*) fiber Bragg grating, (*6*) attenuator, (*7*) optical power combiner, (*8*) optical switch, and (*9*) *p–i–n* diode receiver.

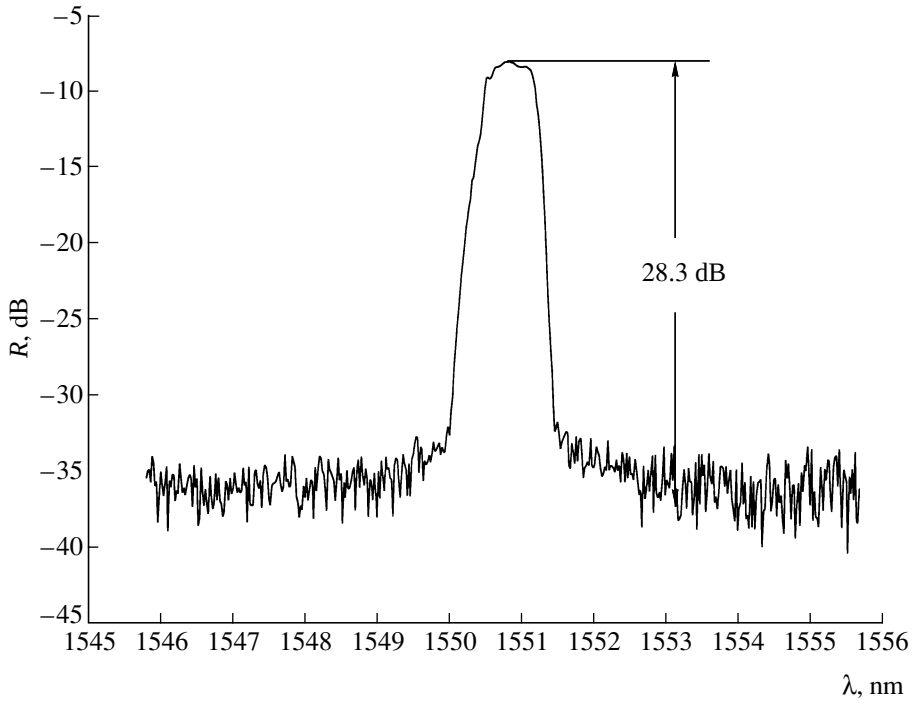

Fig. 6. Reflection spectra of the FBG.

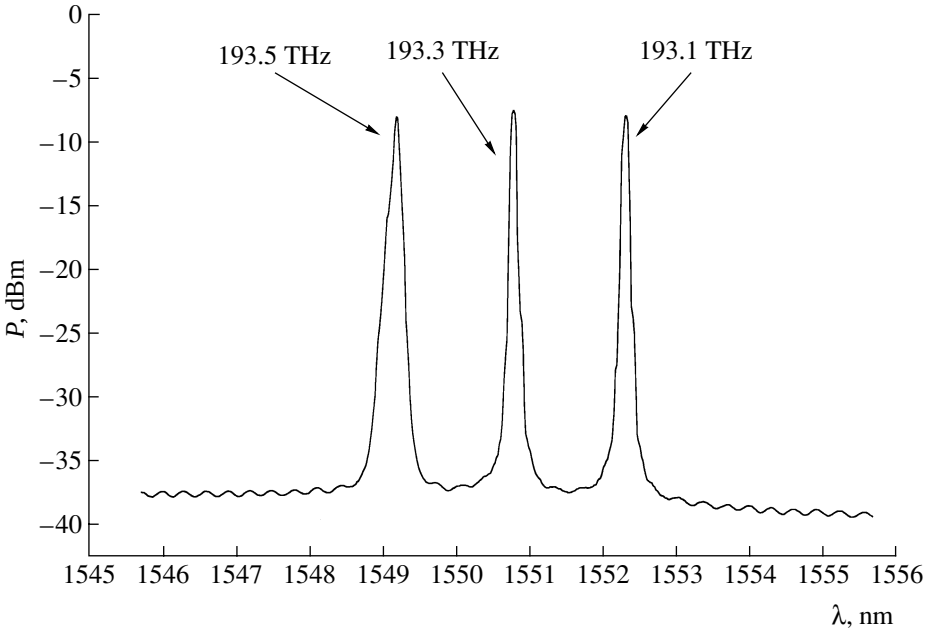

Fig. 7. Input spectra at the OADM.

through the circulator; then the filtered signal is reflected back to the circulator where it is removed. The remaining channels are coupled with the added channel in a power combiner, and after passed by a variable attenuator. The optical switch allows the selection of the add-drop operation by dropping and adding a channel or by pass-through operation adding the previously removed channel again.

To investigate the operation and system performance of this OADM, three distributed feedback lasers (DFB) based at the ITU grid of 200 GHz (≈1.6 nm spacing with wavelengths of 1549.32, 1550.92 (dropped channel), and 1552.52 nm, were externally modulated, through a Ti : $LiNbO_3$ Mach-Zhender intensity modulator, at 2.48832Gbit/s (STM-16), with a nonreturn to zero (NRZ) 2^7–1 pseudorandom bit sequence (PRBS).

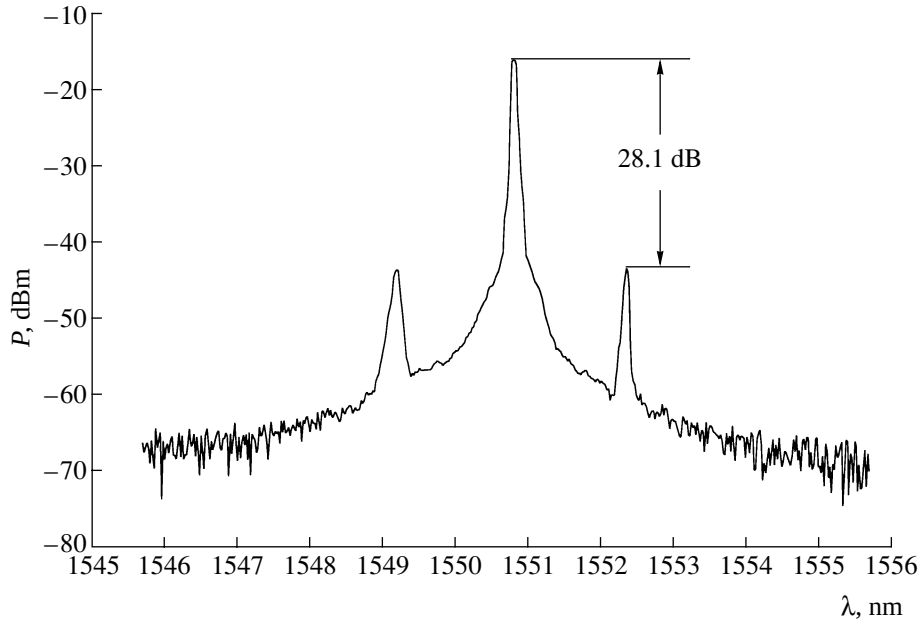

Fig. 8. Spectra of the dropped channel at the OADM.

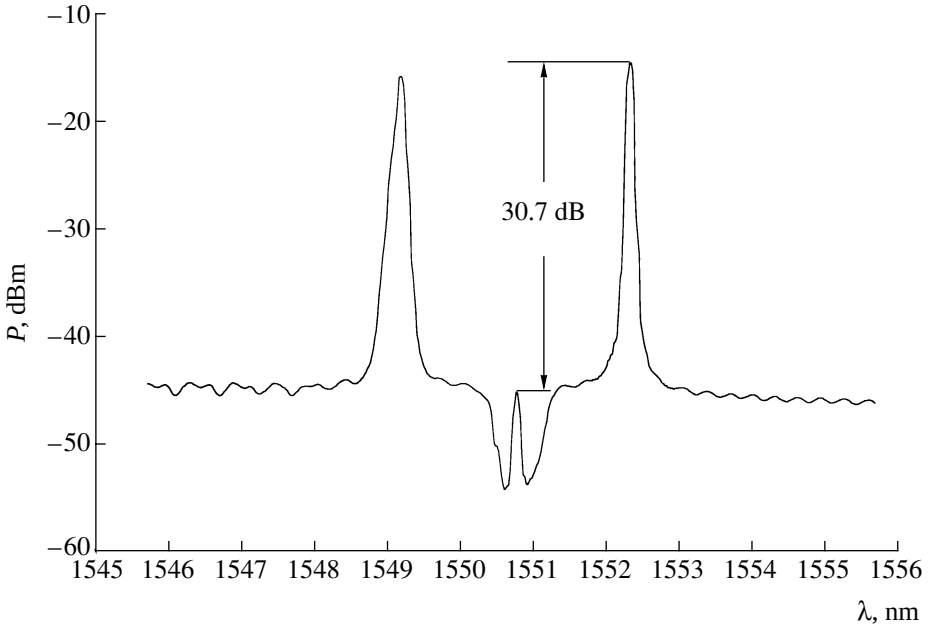

Fig. 9. Spectra of the pass signal on the FBG.

In the experimental transmission link, 75 km of single mode fiber is used. Two Erbium doped fiber amplifiers (EDFA) having saturated output powers of 13 and 17 dBm and noise figures smaller than 4 dB are used to provide the required power to compensate the link and OADM losses.

The average pass-through (dropping and adding of the same signal, without any local processing), added, and drop insertion loss for the dropped channel is 10, 6, and 4 dB, respectively; the insertion loss for the remaining channels is 10 dB. The relatively high insertion losses are due to the power combiner and optical attenuators used to equalize the power of all channels at the OADM output on add-drop or pass-through operation.

The performance of the OADM is related with the spectral characteristics of the fiber Bragg grating. Figure 6 plots the reflection spectra of the FBG coupled to the optical circulator.

The isolation and crosstalk of the optical circulator are greater than 60 dB and the FBG have a central reflective wavelength of 1550.92 nm, with 0.73 and 1.388 nm for the –3 and –20 dB bandwidth, respec-

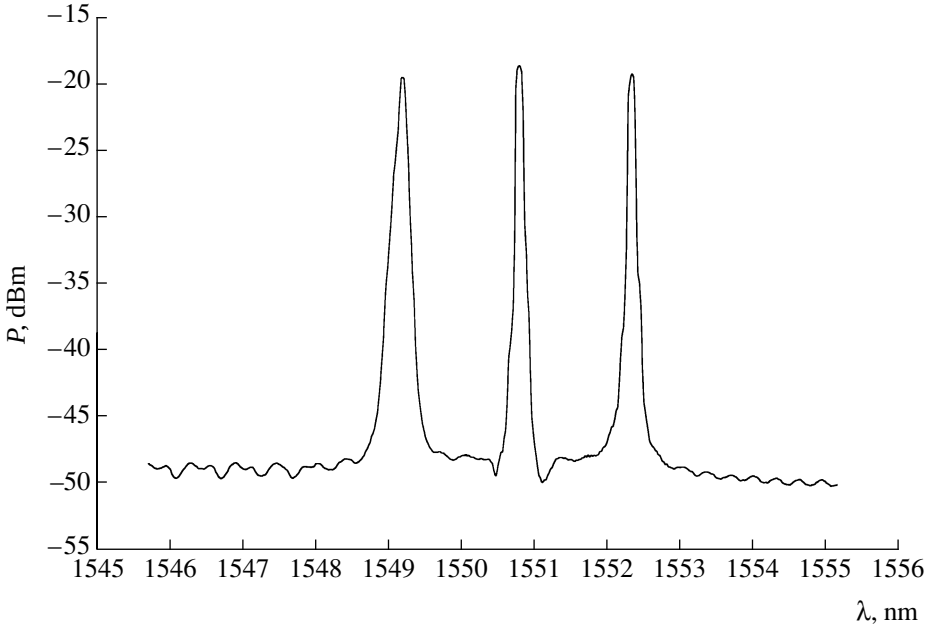

Fig. 10. Output spectra of the OADM.

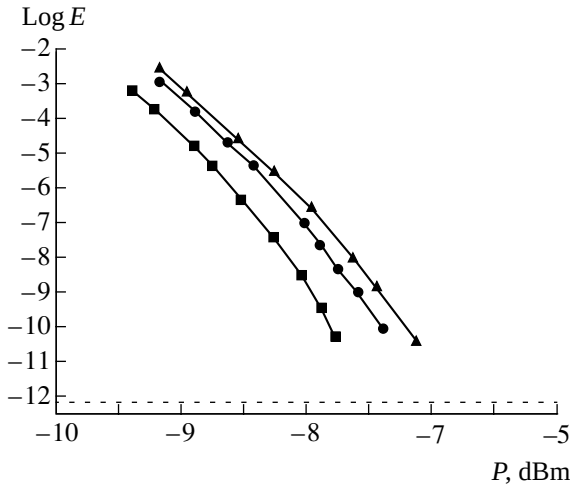

Fig. 11. BER performance against the receiver power for the dropped channel.

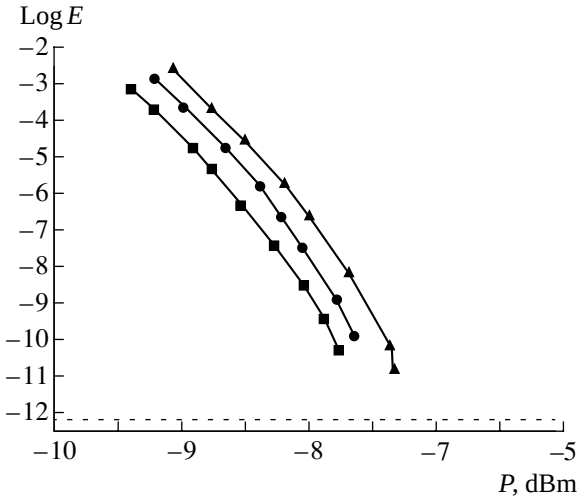

Fig. 12. BER performance against the receiver power for the added channel.

tively. The rejection of the FBG for the adjacent channels is –28.3 dB and the insertion loss to the central wavelength is –30.7, which corresponds to a 99.99% reflectivity.

Figures 7–10 show the spectral characteristics of the OADM, and are the input spectrum, the dropped spectrum, the pass signal on the FBG, and the output spectrum after the insertion of the added channel, respectively.

In Fig. 7, the carrier frequency is indicated on the graph; the central reflection frequency of the grating corresponds to the central channel (193.3 THz). The two small components present with the dropped signal in Fig. 8 are due to residual reflections on the circulator connectors and to the imperfect rejection of the FBG to the adjacent channels; the power of the leakage signals are in agreement with the characteristics of the FBG.

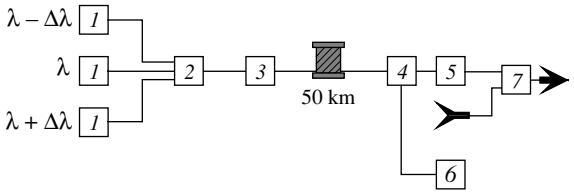

Fig. 13. Setup used to measure the channel spacing power penalty. (*1*) Optical transmitter, (*2*) optical switch, (*3*) optical amplifier, (*4*) circulator, (*5*) fiber Bragg grating, (*6*) *p–i–n* diode receiver, (*7*) optical power combiner.

The theoretical power penalty due to heterodyne crosstalk is obtained using Eq. (1), and this value of crosstalk is 0.01 dB.

The small spectral component at 193.3 THz, which corresponds to the central frequency of the FBG, on the signals of Fig. 9, results from the imperfect reflection of the central wavelength by the FBG. Again, the power of the leakage signal is in agreement with spectral characteristics of the FBG, and the theoretical power penalty due to homodyne crosstalk obtained using Eq. (2) is 0.14 dB.

Figure 10 shows the OADM output signal spectrum. The channel powers are equalized using the attenuator.

Figure 11 shows the BER performance against the receiver power for the back to back operation (0 km), for the dropped channel on the OADM after propagation on 50 km of fiber, and for the dropped channel after propagation on 50 km of fiber; the BER floor is also indicated. The power penalty measured at $E = 10^{-9}$ BER is 0.08 dB.

Figure 12 presents the BER performance against the receiver power for the back to back operation (0 km), for the added channel on the OADM before propagation on 20 km of fiber, and for the dropped channel after propagation on 20 km of fiber; the BER floor is also indicated. The power penalty measured at $E = 10^{-9}$ BER is 0.18 dB.

The power penalty measured in Figs. 11 and 12 are in agreement with the results calculated by Eqs. (1) and (2), within the experimental uncertainties.

The tolerance of the OADM to the channel spacing Δ was investigated. The power penalty due to channel spacing was measured keeping the central wavelength fixed and approaching the other two channels; the power penalty for a channel spacing for which the FBG was designed (200 GHz) was considered 0 dB; the setup used to measure the channel spacing power penalty is seen in Fig. 13.

Figure 14 shows the results of the power penalty; also the full width bandwidth at –1, –3, and –20 dB are shown.

As the channel spacing decreased, the power penalty increases due to heterodyne crosstalk, since the rejection of the FBG to the adjacent channel decreases. Although the OADM had been specified for a channel spacing of 200 GHz, the use of a 100-GHz spacing will increase the power penalty by less than 0.25 dB.

The tolerance of the OADM to the channel detuning was also investigated. The power penalty for the added channel due to the wavelength detuning of the removed and added channel with the central wavelength of the FBG is analyzed; the power penalty for a 0 nm detuning was considered 0 dB; and the setup used to measure the detuning power penalty is shown in Fig. 15.

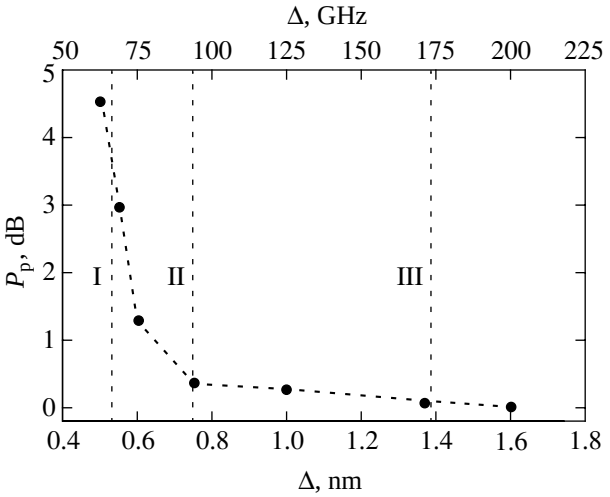

Fig. 14. Power penalty of the removed channel as functions of the channel spacing. Vertical dashed lines *I–III* correspond to the total bandwidths measured at levels of –1, –3, and –20 dB.

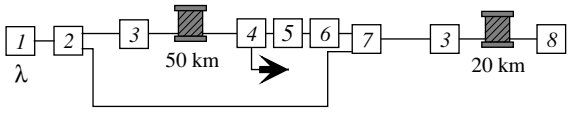

Fig. 15. Setup used to measure the detuning power penalty. (*1*) Optical transmitter, (*2*) optical power divider, (*3*) optical amplifier, (*4*) circulator, (*5*) fiber Bragg grating, (*6*) attenuator, (*7*) optical power combiner, and (*8*) *p–i–n* diode receiver.

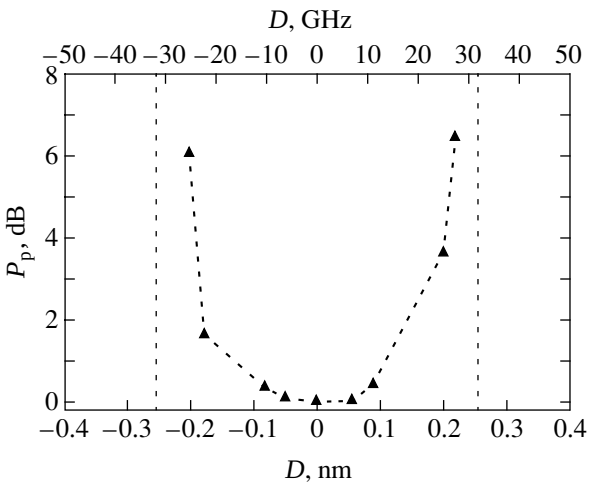

Fig. 16. Power penalty of the removed channel as functions of detuning *D* from the center frequency. The vertical dashed lines correspond to the total bandwidths measured at a level of –0.5 dB.

Figure 16 presents the results of the power penalty; also the full width bandwidth at –0.5 dB are shown.

As the channel detuning between the added channel and the FBG increases, the power penalty increases due to homodyne crosstalk, since the rejection of the FBG

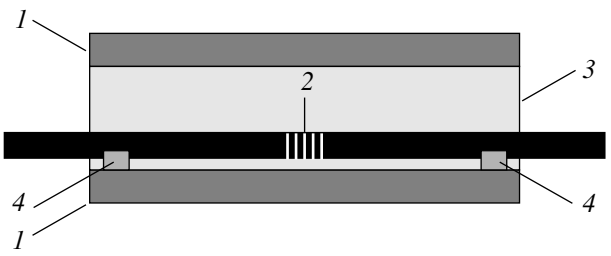

Fig. 17. Enhanced thermal tuning configuration: (Al) aluminum rube: (*1*) aluminum tube, (*2*) fiber Bragg grating, (*3*) thermal conductive compound (TCC), and (*4*) boron spacers.

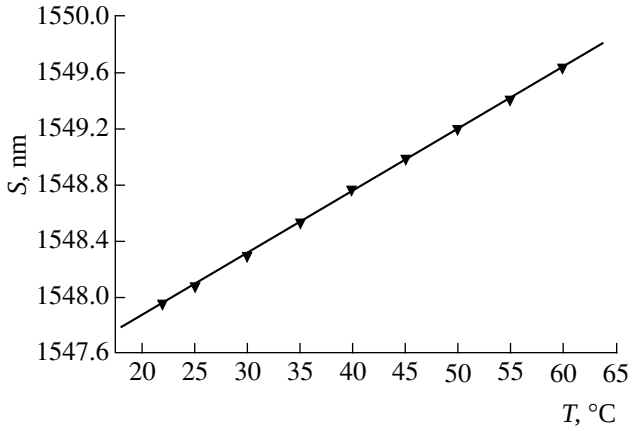

Fig. 18. Dependence of the reflected wavelength on the temperature.

to the central channel decreases. The wavelength tuning of the lasers with the FBG is a crucial aspect to keep the performance of the OADM at a reasonable level, since a detuning of ±0.15 nm results in a power penalty of 0.5 dB to the added channel; this value is considerable if we intend to cascade several OADMs in the network.

IV. TUNABLE OADM

The wavelength tuning capacities of the OADM are related with the FBG capacities to shift their central reflection wavelength. To shift the Bragg grating central wavelength peak, there are two main methods: by modifying the fibre refractive index or by changing the grating period. These variations can be induced thermally or by mechanical stress.

The use of mechanical stress allows a large tuning range (>36 nm) and a high tuning speed (>10 ms/nm), but results in low reproducibility and low reversibility. On the other hand, thermal tuning has high reproducibility, high reversibility, and built-in temperature compensation, but presents a low tuning range (<1 nm) and a low tuning speed (<10 s/nm). We present a hybrid method based on a thermal-stress thermally enhanced actuation on a FBG. The used configuration is schematically illustrated in Fig. 17. The enhancement of the temperature sensitivity of wavelength in this configuration arises from the use of an aluminum tube, which has a positive thermal expansion coefficient, where the FBG is bonded. When heated, the aluminum expands, thereby inducing a strain in the FBG; the temperature also rapidly increases in the FBG due to a thermal conductive compound which fills all the tube and keeps the FBG and the tube in a thermal equilibrium.

The reflection wavelength of an FBG, λ_B, given in expression (3), depends on the effective refraction index of the fiber, n_{eff}, and on the refraction index modulation period, Λ:

$$\lambda_B = 2n_{\text{eff}}\Lambda. \quad (3)$$

Therefore, the variation of the reflection wavelength

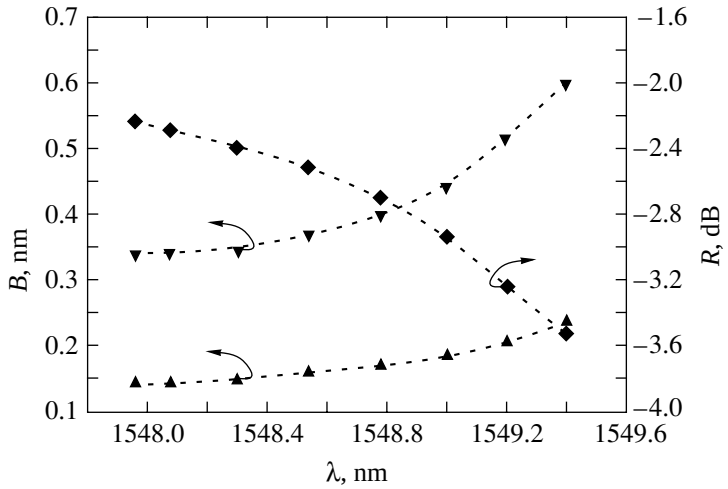

Fig. 19. Spectral characteristics of the FBG with temperature: (triangles with up-oriented vertices) reflection spectrum bandwidth measured at a level of –3 dB, (triangles with down-oriented vertices) reflection spectrum bandwidth measured at a level of –20 dB, and (squares) reflectivity.

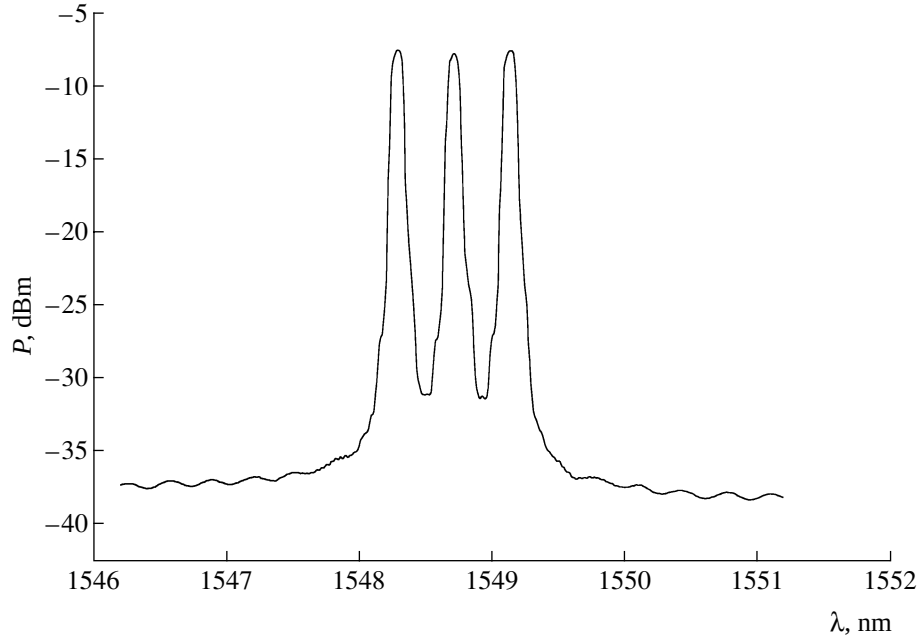

Fig. 20. Input optical spectrum at the OADM.

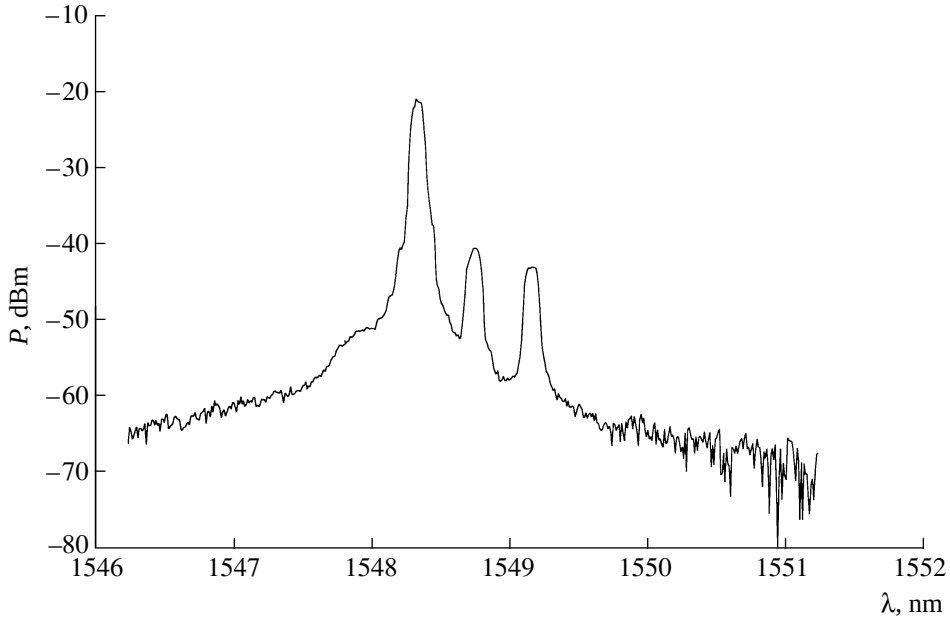

Fig. 21. Optical spectra of the dropped channel 1.

as a function of temperature and stress is

$$\Delta\lambda_B = 2\left(\Lambda\frac{\partial n_{\text{eff}}}{\partial\varepsilon} + n_{\text{eff}}\frac{\partial\Lambda}{\partial\varepsilon}\right)\Delta\varepsilon + 2\left(\Lambda\frac{\partial n_{\text{eff}}}{\partial T} + n_{\text{eff}}\frac{\partial\Lambda}{\partial T}\right)\Delta T. \quad (4)$$

The first term in expression (4) is related to the stress applied to the grating and could be expressed by

$$\Delta\lambda_B(\varepsilon) = \lambda_B(1-p)\varepsilon_z', \quad (5)$$

where p is the photoelastic coefficient of the silica with a value of 0.22, ε_z' is dimensionless stress.

The second term in expression (4) is related to the temperature applied to the grating and could be

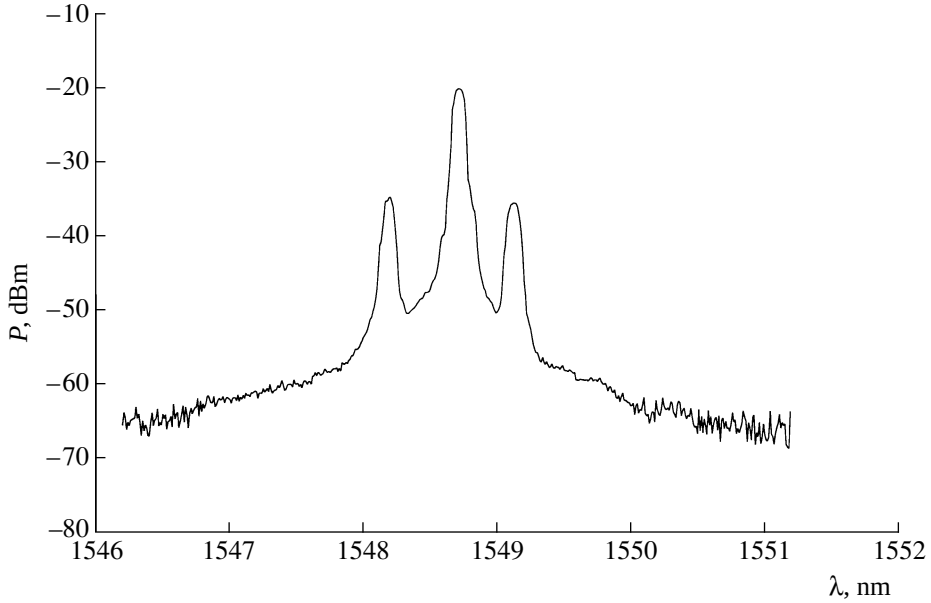

Fig. 22. Optical spectra of the dropped channel 2.

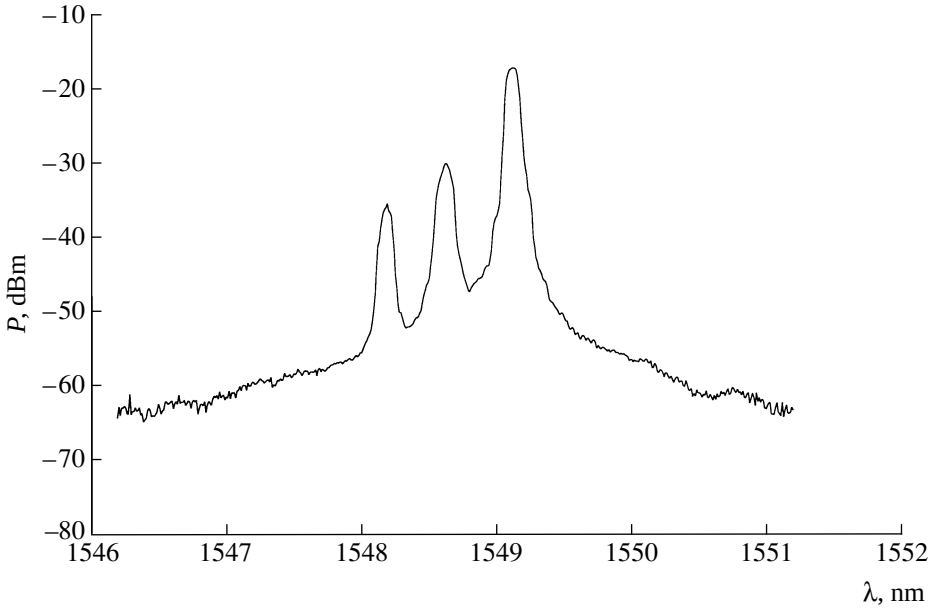

Fig. 23. Optical spectra of the dropped channel 3.

expressed by

$$\Delta\lambda_B(T) = \lambda_B(\alpha_\Lambda + \alpha_n)\Delta T, \quad (6)$$

where α_Λ is the thermal expansion coefficient and α_n is the thermal optic coefficient; in the case of silica, these coefficients have a value of 0.55×10^{-6} and 8.6×10^{-6} °C^{-1}, respectively.

The induced strain on the grating depends on the temperature of the aluminum tube, ΔT, and on the thermal expansion coefficient of the aluminum, which has a value of $\alpha_{CTE} = 22.0 \times 10^{-6}$°C^{-1},

$$\varepsilon_z' = \alpha_{CTE}\Delta T. \quad (7)$$

Substituting expressions (5)–7) into expression (4) we get the following expression for the shift of the FBG reflection wavelength:

$$\Delta\lambda_B = \lambda_B[(1-p)\alpha_{CTE} + (\alpha_\Lambda + \alpha_n)]\Delta T. \quad (8)$$

For a typical wavelength in the region of 1550 nm, the tuning coefficient calculated by expression (8) is 41.1 pm/°C.

Figure 18 shows the dependence of the reflected wavelength on the temperature of the FBG and aluminum tube; from that data, we calculate a value of 44.3 pm/°C for the tuning coefficient.

The increase in temperature and stress applied to the FBG results in a lowering of the reflectivity and an increase in the bandwidth; however, these alterations in the FBG performance do not significantly affect the performance of the OADM. Figure 19 shows the variations of the reflectivity for the –3 and –20 dB bandwidth of the FGB with temperature.

The tunable OADM performance was tested on a three-channel, 50-GHz spaced (193.55, 193.60, and 193.65 THz) DWDM system identical to that shown in Fig. 5. Figure 20 shows the input optical spectrum at the OADM.

Figures 21–23 show the optical spectra of the three removed channels; the temperature of the FBG necessary to tune the system for the removed channels is 30, 40, and 50°C, respectively.

V. CONCLUSIONS

We have reported an OADM solution for DWDM systems using an FBG. The OADM performance was demonstrated in a 200-GHz, 3-channel WDM system working at STM-16 bitrate; the power penalty due to the presence of the OADM in the network is small and, therefore, the cascading capacity of this OADM configuration is high when compared with other OADM configurations [1]. The transparency of the OADM to the channel spacing and number of channels was demonstrated.

The tuning capacity of the OADM based on a thermal-thermal stress enhanced tunable FBG was also demonstrated. This hybrid tuning technique allows us to increase the tuning range and keep the thermal tuning advantages. This hybrid technique can be improved by using a higher thermal expansion coefficient material instead of aluminum.

ACKNOWLEDGMENTS:

Work financed by the Portuguese scientific program PRAXIS XXI through the DAWN project and by Portugal Telecom through the O-NODE project.

REFERENCES

1. Tachikawa, Y., Inoue, Y., Ishii, M., and Nozawa, T., *J. Lightwave Technol.*, 1996, vol. 14, no. 6, p. 977.
2. Oda, K. and Toba, H., *IEEE Photonics Technol. Lett.*, 1993, vol. 5, no. 7, p. 825.
3. Hattori, K., Fukui, M., Jinno, M., *et al.*, *J. Lightwave Technol.*, 1999, vol. 17, no. 12, p. 2562.
4. Chen, Y.-K., Chang, C.-H., Yang, Y.-L., *et al.*, *Opt. Commun.*, 1999, vol. 169, no. 2, p. 245.
5. Andre, P.S., Almeida, T., Pinto, J.L., *et al.*, *Especificacao do OADM, O-Node Project (P114). Report 01/ Phase 1*, 1999.
6. Mizuochi, T., Kitayama, T., Shimizu, K., and Ito, K., *J. Lightwave Technol.*, 1998, vol. 16, no. 2, p. 256.
7. Gimlett, J.L. and Cheung, N., *J. Lightwave Technol.*, 1989, vol. 7, no. 6, p. 888.
8. Mavoori, H., Jin, S., Espindola, R.P., and Strasser, T.A., *Opt. Lett.*, 1999, vol. 22, no. 11, p. 714.
9. Iocco, A., Limberger, H.G., Salathe, R.P., *et al.*, *J. Lightwave Technol.*, 1999, vol. 17, no. 7, p. 1217.